Scientia Iranica A (2020) 27(1), 134–158

Sharif University of Technology
Scientia Iranica
Transactions A: Civil Engineering
http://scientiairanica.sharif.edu

Pulse extraction of pulse-like ground motions based on particle swarm optimization algorithm

S.R. Hoseini Vaez* **and Z. Minaei**

Department of Civil Engineering, Faculty of Engineering, University of Qom, Qom, Iran.

Received 18 November 2017; received in revised form 9 January 2018; accepted 18 June 2018

KEYWORDS
Pulse-like records; Mathematical simulation; Velocity pulse; Particle Swarm Optimization (PSO); Penalty function.

Abstract. Considering the devastating effects of near-fault earthquakes, seismologists and engineers have, qualitatively and quantitatively, represented the strong velocity pulse of near-fault ground motions using models including physical parameters associated with the wave propagation process. In some mathematical models, the derivation of physical parameters is required to fit time history and response spectrum of the simulated record to the actual record through a trial-and-error process, which limits the scope of these models. In the current study, the Particle Swarm Optimization (PSO) algorithm is replaced with the trial-and-error procedure. In this way, an automatic and quantitative process with the minimal judgment of the analyst is prepared to extract a wide range of pulse-like records. Then, the proposed approach is applied to simulate and represent mathematically a set of 91 pulse-like records from the Next Generation Attenuation (NGA) project ground motion library. The obtained results show that a velocity pulse of each pulse-like record could be extracted using the proposed approach; therefore, it can be considered as a powerful tool in pulse parametric studies and the relationship between velocity pulse and structure's response.

1. Introduction

In the vicinity of causative faults, when a fault ruptures towards the station with a velocity close to the shear wave velocity, significant seismic energy is often released as a pulse at the beginning of velocity time history. These pulse-like motions have a significant structural damage potential and impose considerable demand on the structure, which cannot be predicted through conventional methods such as elastic-response spectra [1–9].

Because of the destructive effects of such earthquakes, many engineers and seismologists have focused on the quantitative identification and simulation of records containing pulse and studying of structural response to pulse-like motions [10–20]. Baker proposed a criterion for classification of records as pulse-like using wavelet analysis and extracted the largest velocity pulse of these ground motions [21]. To create models that can reliably describe the impulse feature of near-fault motions, Mavroeidis and Papageorgiou [22] and Hoseini Vaez et al. [23] suggested simple mathematical models using unambiguous physical parameters and simulated a set of near-fault records and their corresponding elastic-response spectra. The values of input parameters in the mathematical model are determined by simultaneously fitting its acceleration, velocity, displacement time histories, and the corresponding elastic-response spectra to actual near-fault record based on the trial-and-error process. Recently, Mimoglou et al. [24] determined the parameters of the Mavroeidis and Papageorgiou [22] wavelet by trying

*. *Corresponding author. Fax: +98 2532854228*
E-mail addresses: hoseinivaez@qom.ac.ir (S.R. Hoseini Vaez); z.minaei@stu.qom.ac.ir (Z. Minaei)

doi: 10.24200/sci.2018.5607.1374

the pulse parameters in the possible intervals with a specific step. Such a trial-and-error process limits the ability of researchers and engineers to apply these models and examine their effects on research and practical applications because it is actually possible to identify only a limited number of near-field records, and a large number of pulse-like records cannot be extracted in such a time-consuming process.

The application of metaheuristic algorithms, including the Particle Swarm Optimization algorithm (PSO), has been expanded in solving inverse problems and structural optimizations [25–30]. PSO algorithm is a swarm intelligence algorithm based on the social behavior of birds or fish which has been practically used in many research fields due to easy implementation and the algorithm's fast convergence speed [31]. This study focuses on PSO algorithm to simultaneously minimize the difference between the time history and the corresponding elastic-response spectra of the model and those of the actual record. Thus, by applying the optimization algorithm, the largest velocity pulse of the pulse-like ground motions is identified and extracted, and an automatic and quantitative process with the minimal judgment replaces the manual trial-and-error method for processing a wide range of records.

2. Simulation models of near-fault ground motions

The model presented by Hoseini Vaez et al. is one of the mathematical models for simulating the strong velocity pulse of near-fault ground motions containing two parts, including both harmonic and polynomial expressions, as shown in Eq. (1) [23]. This model has the capability to simulate various kinds of pulses including unidirectional pulses. Based on Eq. (1), shown in Box I, displacement and acceleration time histories can also be derived in closed form. In Eq. (1), $V(t)$ is the velocity time history, A is the signal amplitude controller, f_p is the prevailing frequency, ν is the phase difference, γ represents the oscillatory characteristic of the signal, and t_0 denotes the time corresponding to the enveloped peak. The model has been fitted using a trial-and-error procedure with some near-fault pulse records in the Next Generation Attenuation (NGA) project library and has simulated the long-period portion of near-fault records with high accuracy. To specify the values of model input parameters, f_p has first been determined in a way that pseudo-velocity response spectra of the proposed model and the actual record are almost in an identical period. Phase and time window parameters are determined based on the fitting maximum pulse amplitude and velocity record amplitude in the time window. Then, parameter A has been selected as the pulse amplitude controller parameter by taking into account the amplitude of the actual velocity record and the maximum pseudo-velocity response spectrum. Finally, γ parameter, considering its effect on the pulse duration, the number of cycles, and the amplitude of pseudo-velocity response spectrum are specified so that the simulated pulse and the actual record fit desirably [23]. Such a trial-and-error procedure limits the ability of engineers and seismologists to simulate pulse-like near-fault records by using the analytical model. Hence, it is necessary for the trial-and-error process to be replaced by the systematic procedure with the minimal judgment of the analyst.

3. The optimization algorithm

3.1. PSO algorithm

PSO algorithm, developed by Eberhart and Kennedy, is a randomized algorithm based on population in swarm intelligence and is inspired by the social behavior of birds and fish [32,33]. Similar to many optimization algorithms, the PSO method begins with an initial random population as a set of potential solutions. Each element of the population is called a particle. Each particle moves in space based on its own experience and that of other particles. During the optimization process, the best personal experience of each particle and the group's best experience are stored in the algorithm's memory and, by using these data, particle's velocity and position are updated according to Eqs. (2) and (3). Thus, with the repetition of particle movement in space, the knowledge of a good solution is retained by all particles; feasible space is searched, and then the optimal response is found based on personal and collective information.

$$V_i^{k+1} = wV_i^k + c_1 r_1 (Pbest_i^k - X_i^k) + c_2 r_2 (Gbest^k - X_i^k), \quad (2)$$

$$X_i^{k+1} = X_i^k + V_i^{k+1}, \quad (3)$$

$$V(t) = \begin{cases} A\left(\frac{4f_p}{\gamma}\right)^4 \left((t-t_0)^2 - \left(\frac{\gamma}{4f_p}\right)^2\right)^2 \cos(2\pi f_p t + \nu), & (t_0 - \frac{\gamma}{4f_p}) \le t \le (t_0 + \frac{\gamma}{4f_p}), \quad \gamma \ge 1 \\ 0, & \text{otherwise} \end{cases} . \quad (1)$$

Box I

where k is the iteration number, V_i is the velocity of the ith particle, X_i is the position of the ith particle, $Pbest_i$ is the best position of the ith particle, and $Gbest$ is the best particle among all the particles in the population; c_1 and c_2 are the learning factors called cognitive parameter and social parameter, respectively; r_1 and r_2 are the random numbers with uniform distribution at the interval [0,1]; w is the local and global exploration controller of the search space, which is called inertia weight and is expressed as the linear reduction function, as in Eq. (4) [31]:

$$w = w_{\max} - \frac{w_{\max} - w_{\min}}{k_{\max}} k, \tag{4}$$

where $w_{\max}$ and $w_{\min}$ are the maximum and minimum inertia weights, $k_{\max}$ is the number of algorithm iterations, and k is the current number of iteration, respectively.

3.2. The penalty function method

Optimization problems often have constraints that must be satisfied in the optimization process, as defined in the following general form [34]:

$$\text{Min} f(x)\ x = (x_1, \cdots x_n) \in S \subseteq R^n, \tag{5}$$

subject to:

$$\begin{array}{ll} g_p(x) \leq 0 & p = 1, 2, ..., P, \\ h_q(x) = 0 & q = 1, 2, ..., Q, \end{array} \tag{6}$$

where $f(x)$, $g_p(x)$, $h_q(x)$, and x are the objective function, the pth inequality constraint, the qth equality constraint, and the n-dimensional vector of decision variables, respectively, and S is the feasible region restricted to the lower and upper boundaries of parameters.

Different methods have been developed by researchers to satisfy the constraints in the optimization algorithms, and among these, the penalty function method is the most popular one. From a theoretical and a numerical point of view, the penalty function solves constrained problems by adding value to the objective function proportional to the constraint violation value as in the following:

$$F(x) = f(x) + \left[\sum_{p=1}^{P} c_p G_p + \sum_{q=1}^{Q} c_q H_q \right], \tag{7}$$

where F is the new objective function to be optimized, and c_p and c_q are penalty parameters. G and H are the functions of g and h constraints, respectively, to calculate the violation of inequality and equality constraints and are defined as follows:

$$G_p = \max\left[g_p(x), 0\right]^{\beta}, \qquad p = 1, 2, ..., P, \tag{8}$$

$$H_q = |h_q(x)|^{\gamma}, \quad q = 1, 2, ..., Q, \tag{9}$$

where γ and β are usually 1 or 2. Therefore, if there is a constraint violation, a positive value is added to the objective function and the algorithm reiterates the previous steps to find the potential solution [35].

4. The use of an optimization algorithm to simulate the pulse-like motions

4.1. Introduction of the proposed approach

As mentioned earlier, the strong velocity pulse of pulse-like ground motions is estimated using the mathematical simulation model through a trial-and-error process and by fitting the displacement, velocity, acceleration time histories, and the corresponding elastic-response spectra obtained through the mathematical model and the actual record. In this study, the trial-and-error process is replaced by a new approach, and to best fit the actual elastic-response spectra and the simulated pulse spectrum, the root-mean-square difference between the two spectra is minimized through the PSO algorithm. In addition, to fit the time histories, the root-mean-square difference between the time history of the actual record and that of the proposed model is considered as the constraint in the optimization process. The penalty function method is used to change the constrained optimization algorithm to a non-constrained algorithm. Thus, the objective function is defined as in Eq. (10) and Figure 1, while gray and black lines display the pseudo-velocity response spectra and velocity time histories of the actual record and simulated pulse, respectively.

$$F(x) = \text{RMS}(SV_{\text{Target}} - SV_{\text{Pulse}}) + cH, \tag{10}$$

where RMS is the Root Mean Square value, SV_{Target} and SV_{Pulse} are the pseudo-velocity response spectra of the actual record and the simulated pulse, respectively, c is the penalty parameter, and H indicates the constraint function as follows:

$$H = \begin{cases} \text{RMS}(V_{\text{Target}}(t) - V_{\text{Pulse}}(t)), \\ \qquad \text{when the constraint is violated} \\ 0, \qquad \text{otherwise} \end{cases} \tag{11}$$

where $V_{\text{Target}}(t)$ and $V_{\text{Pulse}}(t)$ are the velocity time histories of the actual record and the simulated pulse, respectively.

Based on the objective function, optimization variables are the input parameters of the model. According to Eq. (1), five optimization variables are A, γ, ν, f_p, and t_0, which bound the upper and lower limits of the search space. In addition, considering the characteristics of pulse-like records from the perspective of seismic movements and improving the optimization process performance, constraints were imposed on the generation of a random initial population and particle movement as follows:

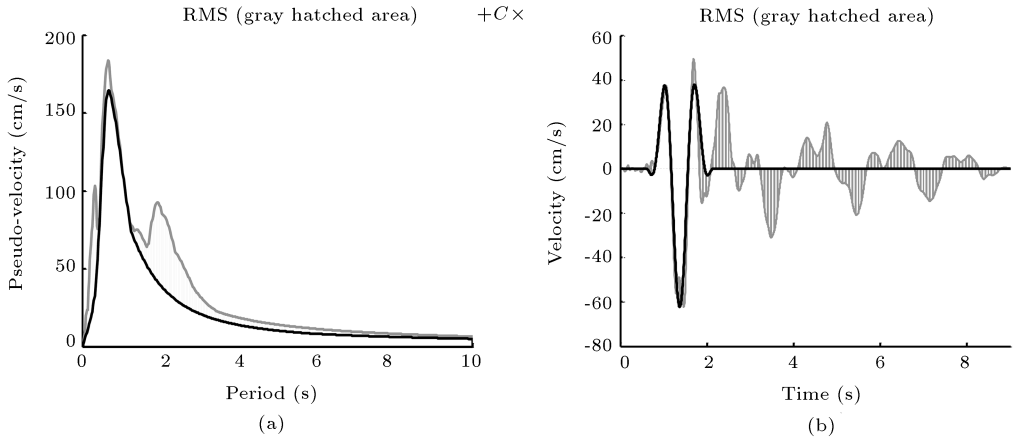

Figure 1. The RMS difference between: (a) The pseudo-velocity response spectra of the actual record and the simulated pulse (gray hatched area) and (b) the velocity time histories of the actual record and the simulated pulse (gray hatched area).

Table 1. The feasible search space of design variables.

Variable	A	ν	γ	f_p	t_0
Search space	[0.3PGV, PGV]	[0,2π]	[4,6]	[0.6FA, FA]	$[t_{PGV} - 20\Delta t, t_{PGV} + 20\Delta t]$

1. The Cumulative Squared Velocity (CSV) of ground motions as a seismic parameter affecting the extraction of the strong velocity pulse is defined as in Eq. (12) [36–38]:

$$CSV(t) = \int_{t_1}^{t_2} V^2(t)dt, \tag{12}$$

where t_1 and t_2 are the starting and ending time points of the velocity time history, respectively. In this study, it is assumed that the energy content of the extracted pulse is smaller than or equal to the actual record. Hence, in the process of generating a random initial population, particles with higher pulse energy content than that of the actual record were not generated. Moreover, particles move in space under this constraint, and if it is not satisfied, particles make a new movement in the search space;

2. In this study, to best fit the actual elastic-response spectra and the simulated pulse spectrum, it is assumed that the simulated pulse spectrum in each period is not larger than the actual record spectrum by more than 5%, and generating a random initial population and particle movement in space should satisfy this condition, too. The flowchart of the proposed approach is shown in Figure 2.

4.2. Results and discussion

4.2.1. Design variables

By studying a wide variety of recorded ground motions and considering research conducted by Hoseini Vaez et al. [23], the search space of design variables is presented in Table 1. Variable A is a coefficient of Peak Ground Velocity (PGV) as in [0.3PGV, PGV] and ν in [0,2π]. According to Eq. (1), a combination of γ and f_p parameters specifies the length of time window. Therefore, to determine the time window length, γ is in [4,6]. Since f_p depends on the frequency content of the actual earthquake records and due to the proximity of Fourier amplitude spectrum in two frequencies, interval [0.6FA, FA] is adopted as the prevalent frequency zone, where FA is the maximum Fourier Amplitude. Figure 3 demonstrates the Fourier spectra and the prevalent frequency zone of the 1971 San Fernando earthquake, Pacoima dam (upper left abut). Variable t_0 is chosen in $[t_{PGV} - 20\Delta t, t_{PGV} + 20\Delta t]$, where t_{PGV} is the occurrence time of PGV and Δt is the recorded ground motion time step. The defined ranges presented in Table 1 create a five-dimensional feasible space and, during optimization, particles are prevented from moving outside this space.

4.2.2. Estimating the strong velocity pulse in the mathematical form

For this study, a wide range of ground motions including 91 NGA records classified as pulse-like by Baker have been investigated [21]. Table 2 presents the specifications of the records. By implementing the proposed approach and the model suggested by Hoseini Vaez et al. [23], the strong velocity pulse of these motions is extracted and represented mathematically.

PSO algorithm parameters are presented in Table 3. The highest velocity pulse in all records is

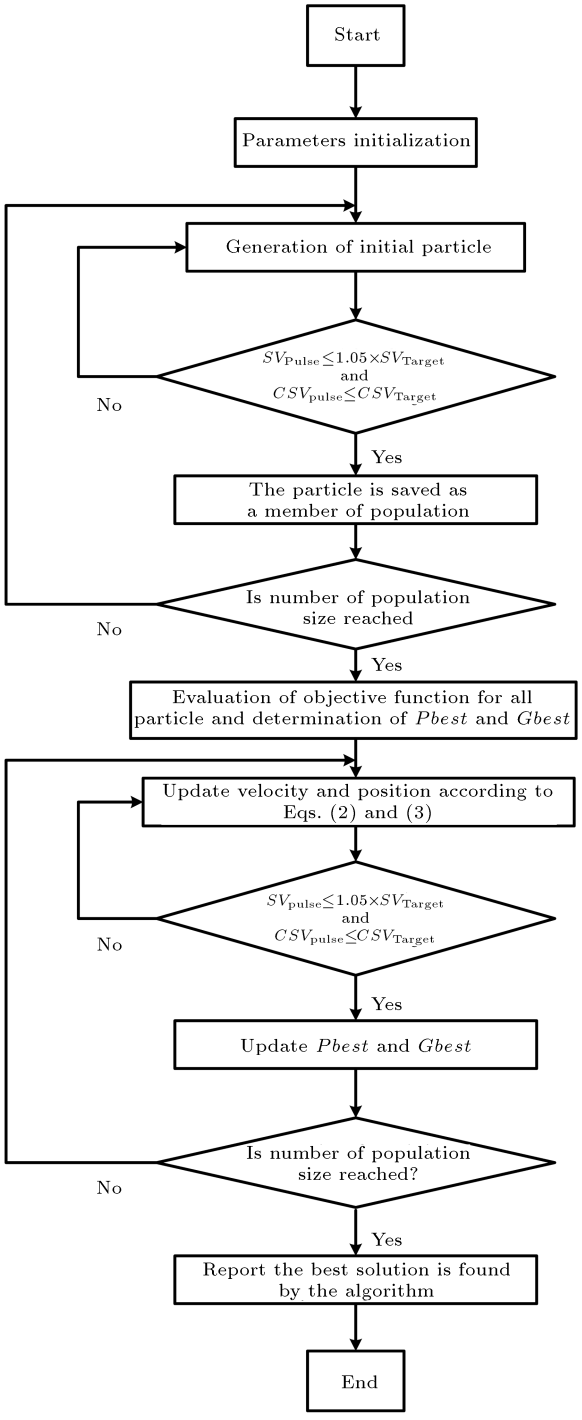

Figure 2. Flowchart demonstration of the proposed approach based on the optimization approach.

extracted using the proposed approach, and the results include parameters A, γ, ν, f_p, and t_0, as shown in Table 4. Complete fitting of the simulated pulse and the actual pulse in all pulse-like records is conducted by substituting the parameters of Table 4 in Eq. (1) (see Appendix A).

By using the input parameters in Table 4, the mathematical model fits the displacement, velocity, acceleration time histories, and the corresponding elastic-response spectra of the actual record. In Figure 4, several extracted strong velocity pulses and the original records are shown, and the complete set is also prepared in Appendix A. In addition, the tripartite logarithmic response spectra of a single degree of freedom oscillator with a 5% damping ratio are illustrated for the extracted pulse and the original record. In these figures, it is observed that the simulated pulse and the actual record are fitted with high quality, and the proposed approach is able to accurately model the long-period portion of the actual record. In addition, the process of convergence to the optimal solution is visible in Figure 5.

4.2.3. The energy content of the strong velocity pulse

In this section, the energy content of the actual record and the simulated velocity pulse are investigated, according to Eq. (12). Table 5 presents the ratio of E_{PR} and E_{Pulse} to E_{Record}, where E_{PR}, E_{Pulse}, and E_{Record} are energy values in the pulse-like region of the actual record, the simulated pulse, and the entire record, respectively. These parameters show that the proposed approach simulates pulse-like records with sufficient accuracy for all records in Table 2. Figure 6 illustrates the energy function of the simulated pulse and the actual record for events, as mentioned in Figures 4 and 5.

4.2.4. The prevalent pulse period

Several methods have been proposed by researchers to determine the velocity pulse period, which is an important parameter for structural engineers. Many researchers consider the zero crossing of the velocity pulse for determining the pulse period, whereas others have used the peak velocity response spectrum. This article defines the pulse period as the inverse of the prevalent frequency of the simulated pulse obtained through the analytical model. This definition is consistent with the physical aspects of the problem and is expressed as in Eq. (13):

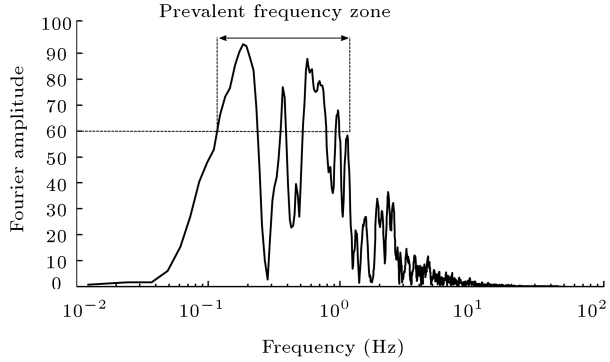

Figure 3. The prevalent frequency zone of the 1971 San Fernando earthquake, Pacoima dam (upper left abut).

Table 2. Pulse-like ground motions in the NGA database [21].

No.	Event	Year	Station name	M_w[a]	PGV (cm/s)	Distance	
						Closest[b] (R)	Epicentral[c]
1	San Fernando	1971	Pacoima Dam (upper left abut)	6.6	116.5	1.8	11.9
2	Coyote Lake	1979	Gilroy array #6	5.7	51.5	3.1	4.4
3	Imperial Valley-06	1979	Aeropuerto Mexicali	6.5	44.3	0.3	2.5
4	Imperial Valley-06	1979	Agrarias	6.5	54.4	0.7	2.6
5	Imperial Valley-06	1979	Brawley Airport	6.5	36.1	10.4	43.2
6	Imperial Valley-06	1979	EC County Center FF	6.5	54.5	7.3	29.1
7	Imperial Valley-06	1979	EC Meloland Overpass FF	6.5	115.0	0.1	19.4
8	Imperial Valley-06	1979	El Centro array #10	6.5	46.9	6.2	26.3
9	Imperial Valley-06	1979	El Centro array #11	6.5	41.1	12.5	29.4
10	Imperial Valley-06	1979	El Centro array #3	6.5	41.1	12.9	28.7
11	Imperial Valley-06	1979	El Centro array #4	6.5	77.9	7.1	27.1
12	Imperial Valley-06	1979	El Centro array #5	6.5	91.5	4.0	27.8
13	Imperial Valley-06	1979	El Centro array #6	6.5	111.9	1.4	27.5
14	Imperial Valley-06	1979	El Centro array #7	6.5	108.8	0.6	27.6
15	Imperial Valley-06	1979	El Centro array #8	6.5	48.6	3.9	28.1
16	Imperial Valley-06	1979	El Centro differential array	6.5	59.6	5.1	27.2
17	Imperial Valley-06	1979	Holtville Post Office	6.5	55.1	7.7	19.8
18	Mammoth Lakes-06	1980	Long Valley Dam (Upr L abut)	5.9	33.1	–	14.0
19	Irpinia, Italy-01	1980	Sturno	6.9	41.5	10.8	30.4
20	Westmorland	1981	Parachute test site	5.9	35.8	16.7	20.5
21	Coalinga-05	1983	Oil City	5.8	41.2	–	4.6
22	Coalinga-05	1983	Transmitter Hill	5.8	46.1	–	6.0
23	Coalinga-07	1983	Coalinga-14th & Elm (old CHP)	5.2	36.1	–	9.6
24	Morgan Hill	1984	Coyote Lake Dam (SW abut)	6.2	62.3	0.5	24.6
25	Morgan Hill	1984	Gilroy array #6	6.2	35.4	9.9	36.3
26	Taiwan SMART1(40)	1986	SMART1 C00	6.3	31.2	–	68.2
27	Taiwan SMART1(40)	1986	SMART1 M07	6.3	36.1	–	67.2
28	N. Palm Springs	1986	North Palm Springs	6.1	73.6	4.0	10.6
29	San Salvador	1986	Geotech investing center	5.8	62.3	6.3	7.9
30	Whittier Narrows-01	1987	Downey - Co Maint Bldg	6.0	30.4	20.8	16.0
31	Whittier Narrows-01	1987	LB - Orange Ave	6.0	32.9	24.5	20.7
32	Superstition Hills-02	1987	Parachute test site	6.5	106.8	1.0	16.0
33	Loma Prieta	1989	Alameda Naval Air Stn Hanger	6.9	32.2	71.0	90.8
34	Loma Prieta	1989	Gilroy array #2	6.9	45.7	11.1	29.8
35	Loma Prieta	1989	Oakland - Outer Harbor Wharf	6.9	49.2	74.3	94.0

[a] Moment magnitude;

[b] Closest distance from the recording site to the ruptured area (if available);

[c] Distance from the recording site to the epicenter.

Table 2. Pulse-like ground motions in the NGA database [21] (continued).

No.	Event	Year	Station name	M_w[a]	PGV (cm/s)	Distance	
						Closest[b] (R)	Epicentral[c]
36	Loma Prieta	1989	Saratoga - Aloha Ave	6.9	55.6	8.5	27.2
37	Erzincan, Turkey	1992	Erzincan	6.7	95.4	4.4	9.0
38	Cape Mendocino	1992	Petrolia	7.0	82.1	8.2	4.5
39	Landers	1992	Barstow	7.3	30.4	34.9	94.8
40	Landers	1992	Lucerne	7.3	140.3	2.2	44.0
41	Landers	1992	Yermo Fire Station	7.3	53.2	23.6	86.0
42	Northridge-01	1994	Jensen Filter Plant	6.7	67.4	5.4	13.0
43	Northridge-01	1994	Jensen Filter Plant Generator	6.7	67.4	5.4	13.0
44	Northridge-01	1994	LA- Wadsworth VA Hospital North	6.7	32.4	23.6	19.6
45	Northridge-01	1994	LA Dam	6.7	77.1	5.9	11.8
46	Northridge-01	1994	Newhall - W Pico Canyon Rd.	6.7	87.8	5.5	21.6
47	Northridge-01	1994	Pacoima Dam (downstr)	6.7	50.4	7.0	20.4
48	Northridge-01	1994	Pacoima Dam (upper left)	6.7	107.1	7.0	20.4
49	Northridge-01	1994	Rinaldi Receiving Sta	6.7	167.2	6.5	10.9
50	Northridge-01	1994	Sylmar - Converter Sta	6.7	130.3	5.4	13.1
51	Northridge-01	1994	Sylmar - Converter Sta East	6.7	116.6	5.2	13.6
52	Northridge-01	1994	Sylmar - Olive View med FF	6.7	122.7	5.3	16.8
53	Kobe, Japan	1995	Takarazuka	6.9	72.6	0.3	38.6
54	Kobe, Japan	1995	Takatori	6.9	169.6	1.5	13.1
55	Kocaeli, Turkey	1999	Gebze	7.5	52.0	10.9	47.0
56	Chi-Chi, Taiwan	1999	CHY006	7.6	64.7	9.8	40.5
57	Chi-Chi, Taiwan	1999	CHY035	7.6	42.0	12.7	43.9
58	Chi-Chi, Taiwan	1999	CHY101	7.6	85.4	10.0	32.0
59	Chi-Chi, Taiwan	1999	TAP003	7.6	33.0	102.4	151.7
60	Chi-Chi, Taiwan	1999	TCU029	7.6	62.3	28.1	79.2
61	Chi-Chi, Taiwan	1999	TCU031	7.6	59.9	30.2	80.1
62	Chi-Chi, Taiwan	1999	TCU034	7.6	42.8	35.7	87.9
63	Chi-Chi, Taiwan	1999	TCU036	7.6	62.4	19.8	67.8
64	Chi-Chi, Taiwan	1999	TCU038	7.6	50.9	25.4	73.1
65	Chi-Chi, Taiwan	1999	TCU040	7.6	53.0	22.1	69.0
66	Chi-Chi, Taiwan	1999	TCU042	7.6	47.3	26.3	78.4
67	Chi-Chi, Taiwan	1999	TCU046	7.6	44.0	16.7	68.9
68	Chi-Chi, Taiwan	1999	TCU049	7.6	44.8	3.8	38.9
69	Chi-Chi, Taiwan	1999	TCU053	7.6	41.9	6.0	41.2

[a]Moment magnitude;

[b]Closest distance from the recording site to the ruptured area (if available);

[c]Distance from the recording site to the epicenter.

Table 2. Pulse-like ground motions in the NGA database [21] (continued).

No.	Event	Year	Station name	M_w[a]	PGV (cm/s)	Distance	
						Closest[b] (R)	Epicentral[c]
70	Chi-Chi, Taiwan	1999	TCU054	7.6	60.9	5.3	37.6
71	Chi-Chi, Taiwan	1999	TCU056	7.6	43.5	10.5	39.7
72	Chi-Chi, Taiwan	1999	TCU060	7.6	33.7	8.5	45.4
73	Chi-Chi, Taiwan	1999	TCU065	7.6	127.7	0.6	26.7
74	Chi-Chi, Taiwan	1999	TCU068	7.6	191.1	0.3	47.9
75	Chi-Chi, Taiwan	1999	TCU075	7.6	88.4	0.9	20.7
76	Chi-Chi, Taiwan	1999	TCU076	7.6	63.7	2.8	16.0
77	Chi-Chi, Taiwan	1999	TCU082	7.6	56.1	5.2	36.2
78	Chi-Chi, Taiwan	1999	TCU087	7.6	53.7	7.0	55.6
79	Chi-Chi, Taiwan	1999	TCU098	7.6	32.7	47.7	99.7
80	Chi-Chi, Taiwan	1999	TCU101	7.6	68.4	2.1	45.1
81	Chi-Chi, Taiwan	1999	TCU102	7.6	106.6	1.5	45.6
82	Chi-Chi, Taiwan	1999	TCU103	7.6	62.2	6.1	52.4
83	Chi-Chi, Taiwan	1999	TCU104	7.6	31.4	12.9	49.3
84	Chi-Chi, Taiwan	1999	TCU128	7.6	78.7	13.2	63.3
85	Chi-Chi, Taiwan	1999	TCU136	7.6	51.8	8.3	48.8
86	Northwest China-03	1997	Jiashi	6.1	37.0	–	19.1
87	Yountville	2000	Napa Fire Station #3	5.0	43.0	–	9.9
88	Chi-Chi, Taiwan-03	1999	CHY024	6.2	33.1	19.7	25.5
89	Chi-Chi, Taiwan-03	1999	CHY080	6.2	69.9	22.4	29.5
90	Chi-Chi, Taiwan-03	1999	TCU076	6.2	59.4	14.7	20.8
91	Chi-Chi, Taiwan-06	1999	CHY101	6.3	36.3	36.0	50.0

[a] Moment magnitude;

[b] Closest distance from the recording site to the ruptured area (if available);

[c] Distance from the recording site to the epicenter.

Table 3. PSO algorithm parameters.

Parameter	Population size	$k_{\max}$	c_1	c_2	$w_{\min}$	$w_{\max}$	c	γ
Value	50	200	2	2	0.8	1.4	5	1

$$T_p = \frac{1}{f_p}, \tag{13}$$

where T_p is the prevalent pulse period. It should be noted that, in the literature, much attention is devoted to the relationship between the prevalent pulse period and the earthquake magnitude. Figure 7 indicates the prevalent pulse period versus earthquake magnitude based on Eq. (13) and Table 4. In this regard, Eq. (14) is generated from a linear regression analysis of the prevalent pulse period and the earthquake magnitude, very similar to those existing in the literature [21]:

$$\log(T_p) = -2.3 + 0.4M_w. \tag{14}$$

Table 4. Input parameters obtained by fitting the pulse-like records in Table 2 to Hoseini Vaez's model.

No.	Event	Year	Station name	A	γ	ν	f_p	t_0
1	San Fernando	1971	Pacoima Dam (upper left abut)	94.51	4	4.55	0.751	3.09
2	Coyote Lake	1979	Gilroy array #6	37.35	4	0.9	1.06	2.7
3	Imperial Valley-06	1979	Aeropuerto Mexicali	34.93	4	5.66	0.569	5.4
4	Imperial Valley-06	1979	Agrarias	38.54	4	1.82	0.485	7.74
5	Imperial Valley-06	1979	Brawley Airport	28.79	4	0	0.281	7.33
6	Imperial Valley-06	1979	EC county Center FF	41.43	4	3.9	0.25	7.48
7	Imperial Valley-06	1979	EC meloland Overpass FF	79.52	4.006	1.19	0.365	4.91
8	Imperial Valley-06	1979	El Centro array #10	34.55	4	4.42	0.241	7.07
9	Imperial Valley-06	1979	El Centro array #11	17.12	5.102	1.15	0.152	8.69
10	Imperial Valley-06	1979	El Centro array #3	26.89	4	4.32	0.218	8.36
11	Imperial Valley-06	1979	El Centro array #4	66.41	4	5.68	0.236	5.29
12	Imperial Valley-06	1979	El Centro array #5	78.92	4	3.28	0.273	7.41
13	Imperial Valley-06	1979	El Centro array #6	94.13	4	3.41	0.267	5.8
14	Imperial Valley-06	1979	El Centro array #7	73.5	4.072	2.02	0.287	6.04
15	Imperial Valley-06	1979	El Centro array #8	39.92	4.18	5.42	0.22	6.98
16	Imperial Valley-06	1979	El Centro differential array	36.07	4	5.94	0.213	6.86
17	Imperial Valley-06	1979	Holtville Post Office	40.03	4.003	0	0.216	7.28
18	Mammoth lakes-06	1980	Long Valley Dam (Upr L abut)	24.22	4.573	2.76	1.003	5.19
19	Irpinia, Italy-01	1980	Sturno	40.77	4.096	1.47	0.347	8.1
20	Westmorland	1981	Parachute test site	27.58	4	2.5	0.317	11.12
21	Coalinga-05	1983	Oil city	40.61	4	4.69	1.655	2.93
22	Coalinga-05	1983	Transmitter Hill	46.06	5.363	4.04	1.325	3.05
23	Coalinga-07	1983	Coalinga-14th & Elm (old CHP)	34.86	4	0.67	2.575	2.82
24	Morgan Hill	1984	Coyote lake Dam (SW abut)	51.64	5.29	5.34	1.267	3.76
25	Morgan Hill	1984	Gilroy array #6	26.64	5.212	0.71	0.927	5.89
26	Taiwan SMART1(40)	1986	SMART1 C00	30.49	4.147	0.9	0.729	7.36
27	Taiwan SMART1(40)	1986	SMART1 M07	36.12	4	0	0.731	11.71
28	N. Palm springs	1986	North Palm Springs	51.82	4	3.78	0.819	2.84
29	San Salvador	1986	Geotech Investig Center	62.26	4	4.55	1.294	1.38
30	Whittier Narrows-01	1987	Downey - Co Maint Bldg	25.42	5.002	0.96	1.222	5.53
31	Whittier Narrows-01	1987	LB - Orange Ave	25.75	5.16	1.96	1.226	6.09
32	Superstition Hills-02	1987	Parachute Test Site	91.79	4	2.55	0.467	12.31
33	Loma Prieta	1989	Alameda Naval Air Stn Hanger	22.25	4	1.55	0.464	12.29
34	Loma Prieta	1989	Gilroy array #2	37.29	5.211	3.48	0.654	4.02
35	Loma Prieta	1989	Oakland - Outer Harbor Wharf	38.61	4	1.17	0.631	12.96
36	Loma Prieta	1989	Saratoga - Aloha Ave	28.36	4	4.05	0.273	6.36
37	Erzican, Turkey	1992	Erzincan	74.79	4	2.47	0.458	3.45
38	Cape Mendocino	1992	Petrolia	45.07	4	3.87	0.404	3.16
39	Landers	1992	Barstow	19.14	4	5.65	0.14	17.66
40	Landers	1992	Lucerne	78.13	4	6.07	0.208	10.15
41	Landers	1992	Yermo Fire Station	37.91	4	4.86	0.148	18.21
42	Northridge-01	1994	Jensen Filter Plant	64.46	4.547	1.69	0.341	3.32
43	Northridge-01	1994	Jensen Filter Plant Generator	65.31	4.365	1.79	0.336	3.32
44	Northridge-01	1994	LA - Wadsworth VA Hospital North	18.11	4	0.87	0.439	9.72
45	Northridge-01	1994	LA Dam	51.39	4	3.38	0.698	2.9
46	Northridge-01	1994	Newhall - W Pico Canyon Rd.	78.51	4	3.5	0.429	5.43

[a]These records are extracted and simulated in different parameter ranges than those in Table 1.

Table 4. Input parameters obtained by fitting the pulse-like records in Table 2 to Hoseini Vaez's model (continued).

No.	Event	Year	Station name	A	γ	ν	f_p	t_0
47[a]	Northridge-01	1994	Pacoima Dam (downstr)	30.86	4.827	4.78	1.984	3.50
48	Northridge-01	1994	Pacoima Dam (upper left)	88.72	4	6.01	1.191	3.97
49	Northridge-01	1994	Rinaldi receiving Sta	120.96	4	3.43	0.813	2.58
50	Northridge-01	1994	Sylmar - Converter Sta	83.11	4.32	1.38	0.349	3.6
51	Northridge-01	1994	Sylmar - Converter Sta East	61.68	4	1.84	0.332	3.43
52	Northridge-01	1994	Sylmar - Olive View med FF	77.59	4	5.3	0.44	3.97
53	Kobe, Japan	1995	Takarazuka	61.20	4	3.88	0.724	5.36
54	Kobe, Japan	1995	Takatori	132.88	4	3.91	0.639	6.11
55[a]	Kocaeli, Turkey	1999	Gebze	37.80	4	0.55	0.185	7.74
56	Chi-Chi, Taiwan	1999	CHY006	46.99	4	3.7	0.43	34.52
57	Chi-Chi, Taiwan	1999	CHY035	34.67	4.686	2.95	0.662	35.55
58	Chi-Chi, Taiwan	1999	CHY101	58.03	4	0	0.205	38.91
59	Chi-Chi, Taiwan	1999	TAP003	27.15	5.167	2.65	0.333	46.75
60	Chi-Chi, Taiwan	1999	TCU029	54.78	4.309	4.92	0.18	51.19
61	Chi-Chi, Taiwan	1999	TCU031	59.86	4.649	2.25	0.199	53.74
62	Chi-Chi, Taiwan	1999	TCU034	22.91	5.121	6.28	0.138	47.3
63	Chi-Chi, Taiwan	1999	TCU036	55.85	4.042	1.95	0.176	46.73
64	Chi-Chi, Taiwan	1999	TCU038	48.07	4	2.57	0.152	47.28
65	Chi-Chi, Taiwan	1999	TCU040	45.23	4.67	4.96	0.183	47.81
66	Chi-Chi, Taiwan	1999	TCU042	31.43	4	0	0.134	48.15
67	Chi-Chi, Taiwan	1999	TCU046	30.91	4.191	1.45	0.133	39.88
68	Chi-Chi, Taiwan	1999	TCU049	34.33	4	2.07	0.099	37.59
69	Chi-Chi, Taiwan	1999	TCU053	26.78	4	3.19	0.093	36.66
70	Chi-Chi, Taiwan	1999	TCU054	38.67	4	0.63	0.135	36.19
71	Chi-Chi, Taiwan	1999	TCU056	23.86	4	1.26	0.11	38.47
72	Chi-Chi, Taiwan	1999	TCU060	21.88	4.046	0.78	0.083	41
73	Chi-Chi, Taiwan	1999	TCU065	93.45	5.49	3.02	0.207	31.80
74[a]	Chi-Chi, Taiwan	1999	TCU068	191.15	3	1.34	0.082	38.35
75	Chi-Chi, Taiwan	1999	TCU075	72.17	4	3.73	0.213	29.42
76	Chi-Chi, Taiwan	1999	TCU076	39.31	4	3.51	0.262	28.29
77	Chi-Chi, Taiwan	1999	TCU082	39.28	4	1.45	0.133	35.33
78[a]	Chi-Chi, Taiwan	1999	TCU087	31.81	4	4.14	0.111	41.67
79	Chi-Chi, Taiwan	1999	TCU098	26.68	4	5.53	0.158	48.69
80	Chi-Chi, Taiwan	1999	TCU101	39.18	4	3.63	0.146	17.07
81	Chi-Chi, Taiwan	1999	TCU102	57.71	4	1.05	0.159	36.76
82	Chi-Chi, Taiwan	1999	TCU103	54.46	4	4.97	0.135	39.55
83[a]	Chi-Chi, Taiwan	1999	TCU104	25.36	4	0.00	0.083	42.11
84	Chi-Chi, Taiwan	1999	TCU128	72.22	4	2.48	0.177	45.29
85	Chi-Chi, Taiwan	1999	TCU136	36.77	4	4.17	0.113	42.55
86	Northwest China-03	1997	Jiashi	26.55	4	6.28	0.906	5.58
87	Yountville	2000	Napa Fire Station #3	37.86	4	4.78	1.497	13.15
88	Chi-Chi, Taiwan-03	1999	CHY024	32.07	4	0	0.335	13.59
89	Chi-Chi, Taiwan-03	1999	CHY080	66.33	5.379	1.47	0.898	11
90	Chi-Chi, Taiwan-03	1999	TCU076	45.39	4	4	1.179	10.43
91	Chi-Chi, Taiwan-06	1999	CHY101	33.88	4.855	1.19	0.415	25.89

[a]These records are extracted and simulated in different parameter ranges than those in Table 1.

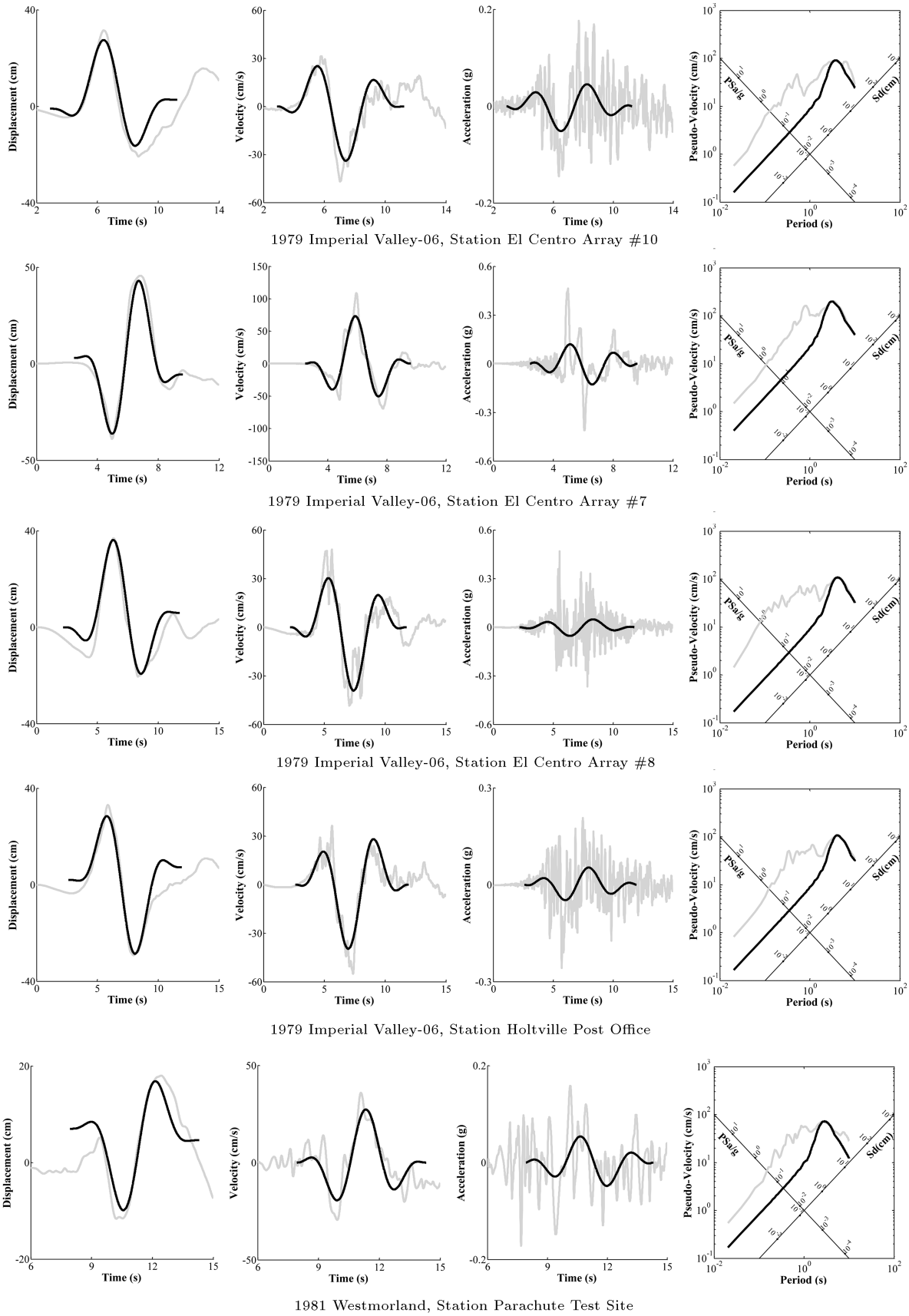

Figure 4. Displacement, velocity, acceleration, and tripartite logarithmic response spectra of actual record (gray) and those of simulated pulse (black) with a 5% damping ratio.

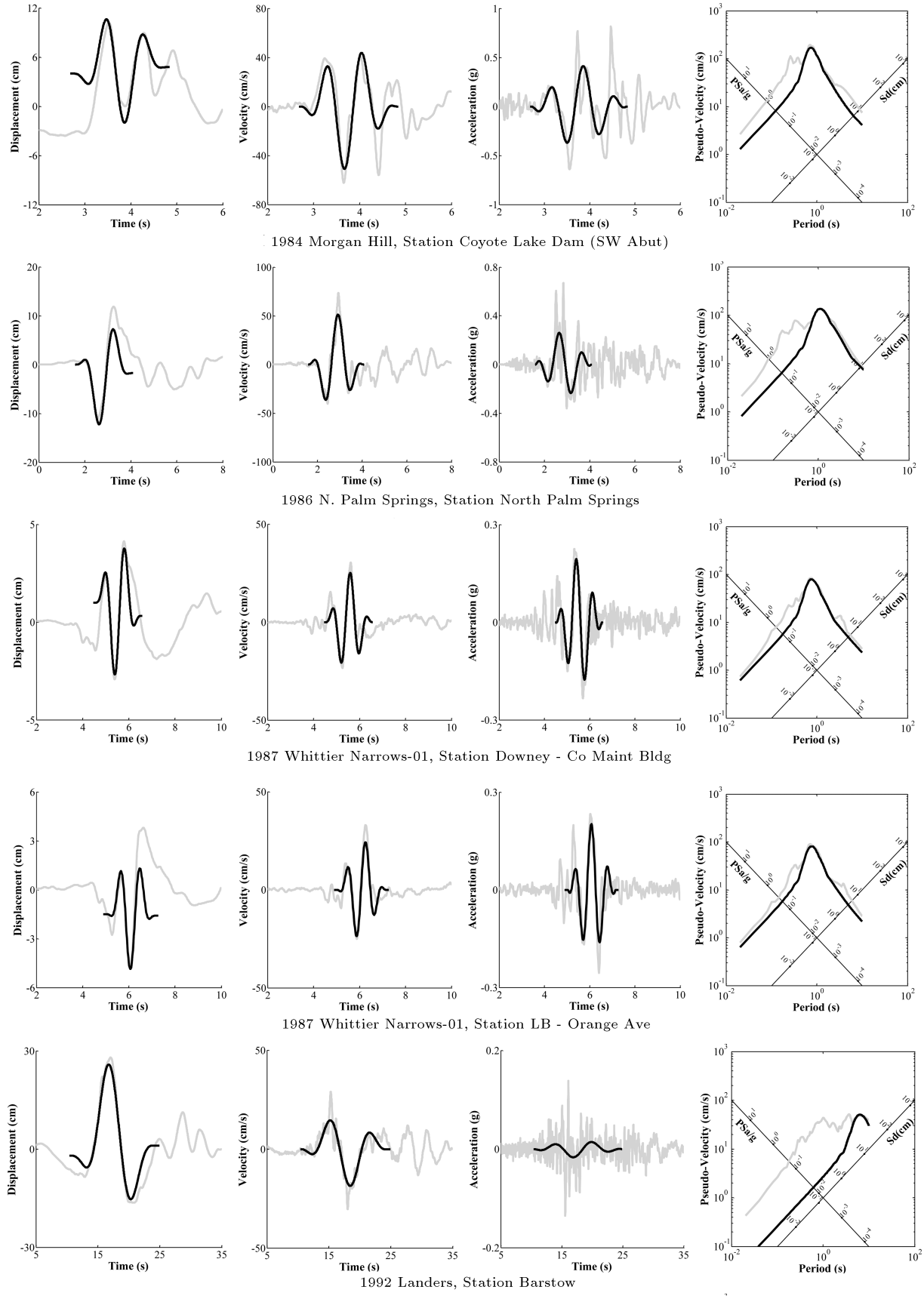

Figure 4. Displacement, velocity, acceleration, and tripartite logarithmic response spectra of actual record (gray) and those of simulated pulse (black) with a 5% damping ratio (continued).

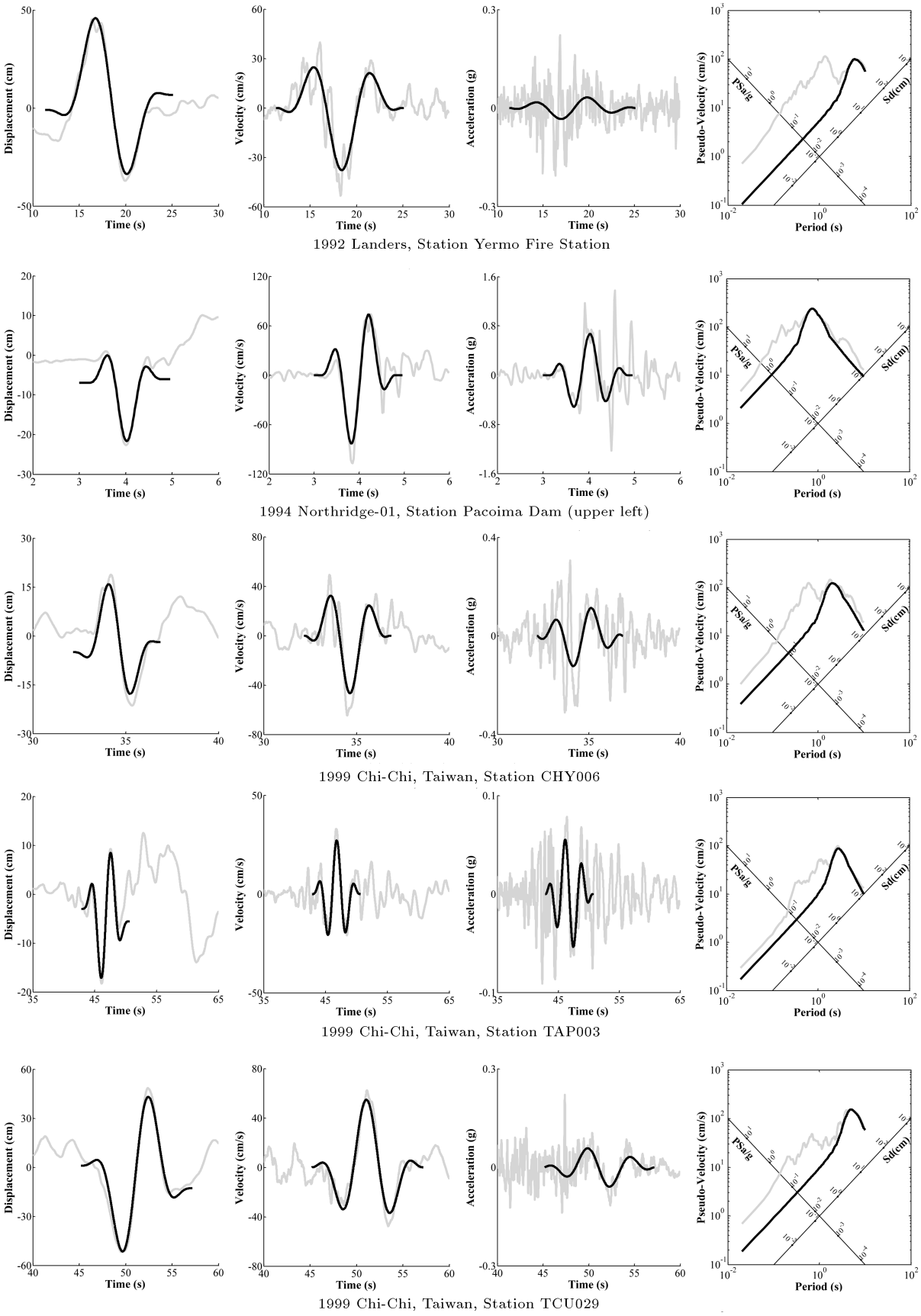

Figure 4. Displacement, velocity, acceleration, and tripartite logarithmic response spectra of actual record (gray) and those of simulated pulse (black) with a 5% damping ratio (continued).

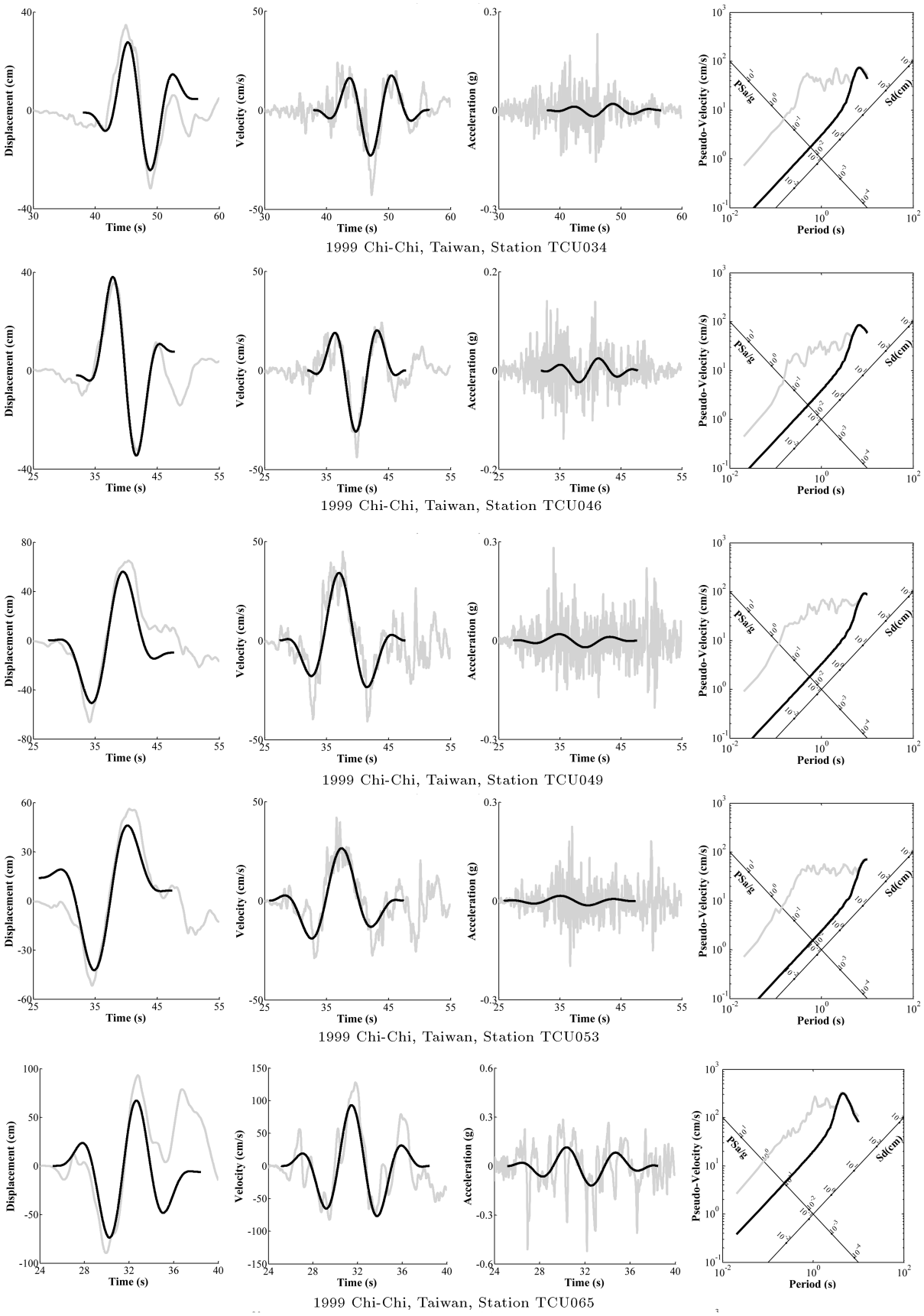

Figure 4. Displacement, velocity, acceleration, and tripartite logarithmic response spectra of actual record (gray) and those of simulated pulse (black) with a 5% damping ratio (continued).

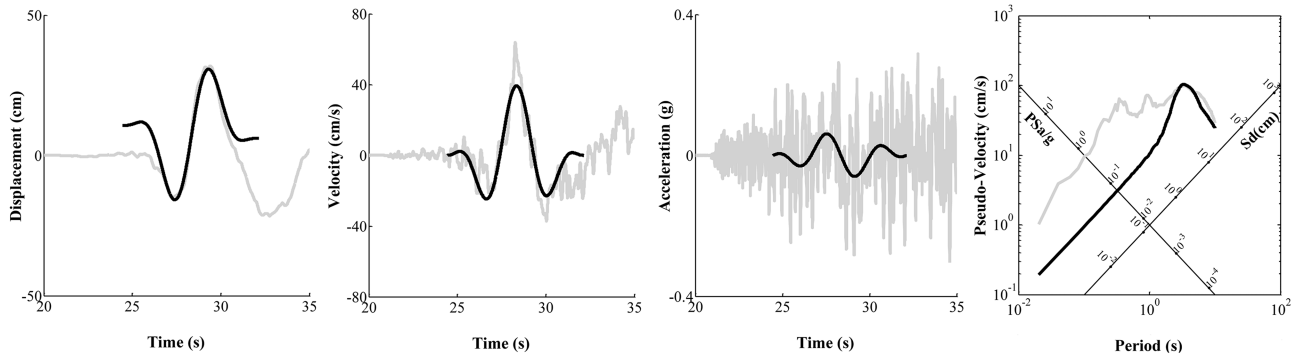

1999 Chi-Chi, Taiwan, Station TCU076

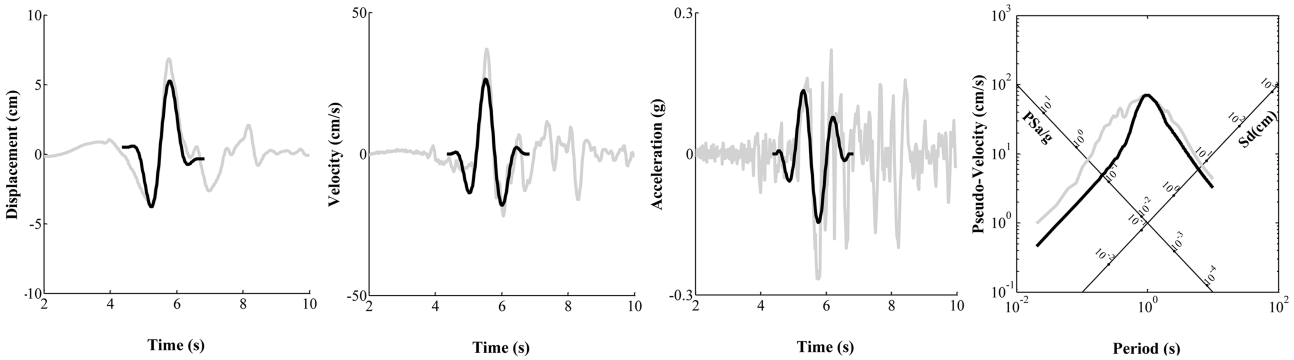

1997 Northwest China-03, Station Jiashi

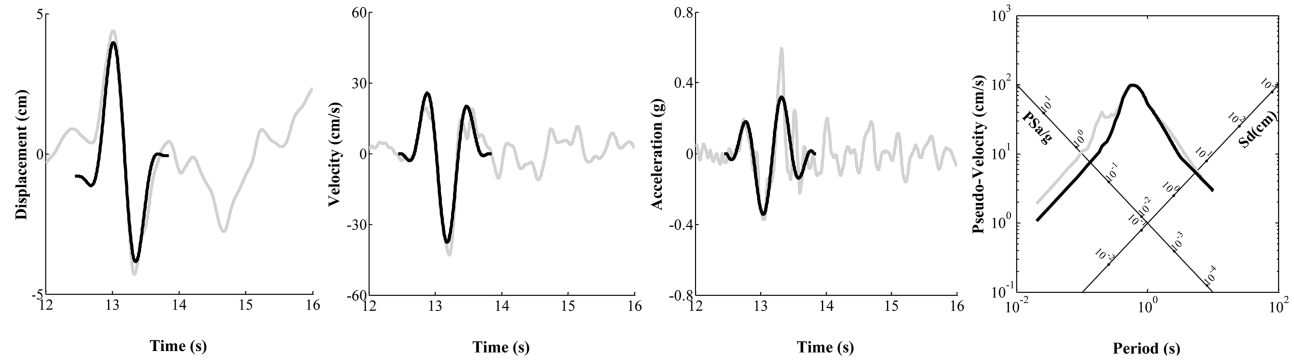

2000 Yountville, Station Napa Fire Station #3

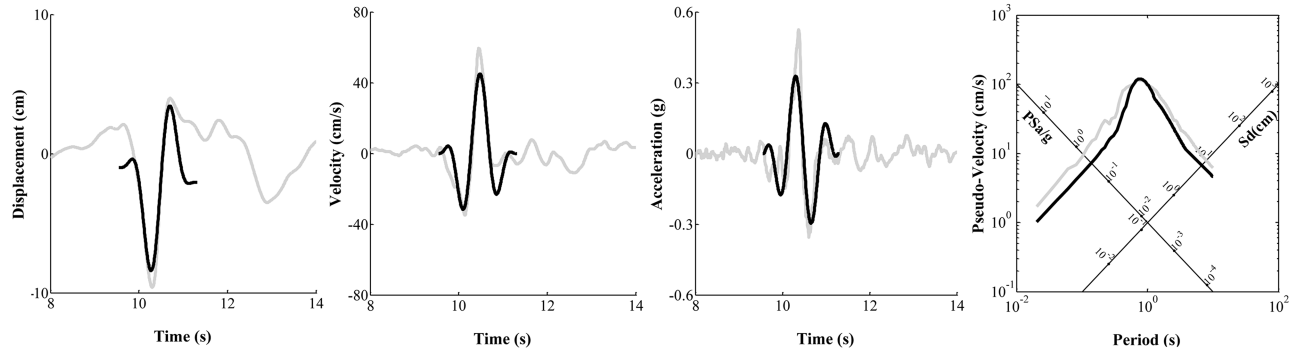

1999 Chi-Chi, Taiwan-03, Station TCU076

Figure 4. Displacement, velocity, acceleration, and tripartite logarithmic response spectra of actual record (gray) and those of simulated pulse (black) with a 5% damping ratio (continued).

Table 5. The comparison between CSV of the actual record and the simulated pulse.

No.	Event	Year	Station name	E_{Record} (cm^2/s)	E_{PR} (cm^2/s)	E_{Pulse} (cm^2/s)	$\frac{E_{\text{PR}}}{E_{\text{Record}}}$	$\frac{E_{\text{Pulse}}}{E_{\text{Record}}}$
1	San Fernando	1971	Pacoima Dam (upper left abut)	9797	5578	4843	0.569	0.494
2	Coyote Lake	1979	Gilroy array #6	760.6	673.9	535.6	0.886	0.704
3	Imperial Valley-06	1979	Aeropuerto Mexicali	1602	944.2	872.7	0.589	0.545
4	Imperial Valley-06	1979	Agrarias	1963	1485	1246	0.756	0.635
5	Imperial Valley-06	1979	Brawley Airport	2105	1384	1202	0.657	0.571
6	Imperial Valley-06	1979	EC County Center FF	4559	3525	2792	0.773	0.612
7	Imperial Valley-06	1979	EC Meloland Overpass FF	9448	8464	7076	0.896	0.749
8	Imperial Valley-06	1979	El Centro array #10	3883	2599	2015	0.669	0.519
9	Imperial Valley-06	1979	El Centro array #11	2042	1690	1001	0.828	0.49
10	Imperial Valley-06	1979	El Centro array #3	2129	1711	1353	0.804	0.636
11	Imperial Valley-06	1979	El Centro array #4	9550	8877	7592	0.930	0.795
12	Imperial Valley-06	1979	El Centro array #5	12194	10740	9285	0.881	0.761
13	Imperial Valley-06	1979	El Centro array #6	15171	14472	13476	0.954	0.888
14	Imperial Valley-06	1979	El Centro array #7	10326	9813	7804	0.950	0.756
15	Imperial Valley-06	1979	El Centro array #8	4316	3886	3083	0.900	0.714
16	Imperial Valley-06	1979	El Centro differential array	4755	4050	2489	0.852	0.524
17	Imperial Valley-06	1979	Holtville Post Office	3890	3480	3021	0.894	0.777
18	Mammoth Lakes-06	1980	Long Valley Dam (Upr L abut)	544.9	376.5	271.5	0.691	0.498
19	Irpinia, Italy-01	1980	Sturno	3184	2188	2000	0.687	0.628
20	Westmorland	1981	Parachute Test Site	2041	1343	975.8	0.658	0.478
21	Coalinga-05	1983	Oil City	827.4	456.5	405.4	0.552	0.49
22	Coalinga-05	1983	Transmitter Hill	1334	1128	872.3	0.846	0.654
23	Coalinga-07	1983	Coalinga-14th & Elm (Old CHP)	328.2	267.3	191.7	0.814	0.584
24	Morgan Hill	1984	Coyote Lake Dam (SW Abut)	1876	1507	1131	0.803	0.603
25	Morgan Hill	1984	Gilroy array #6	730.8	557.2	405.2	0.763	0.554
26	Taiwan SMART1(40)	1986	SMART1 C00	882.2	524.2	538.4	0.594	0.610
27	Taiwan SMART1(40)	1986	SMART1 M07	880.9	713	726	0.809	0.824
28	N. Palm Springs	1986	North Palm Springs	1964	1572	1334	0.800	0.679
29	San Salvador	1986	Geotech Investig Center	2379	1427	1220	0.600	0.513
30	Whittier Narrows-01	1987	Downey - Co Maint Bldg	370.9	315.5	268.5	0.850	0.724
31	Whittier Narrows-01	1987	LB - Orange Ave	478	378.1	283.7	0.791	0.593

Table 5. The comparison between CSV of the actual record and the simulated pulse (continued).

No.	Event	Year	Station name	E_{Record} (cm^2/s)	E_{PR} (cm^2/s)	E_{Pulse} (cm^2/s)	$\frac{E_{\text{PR}}}{E_{\text{Record}}}$	$\frac{E_{\text{Pulse}}}{E_{\text{Record}}}$
32	Superstition Hills-02	1987	Parachute Test Site	12863	9462	7332	0.736	0.57
33	Loma Prieta	1989	Alameda Naval Air Stn Hanger	1029	702.5	434.4	0.683	0.422
34	Loma Prieta	1989	Gilroy array #2	1956	1489	1126	0.761	0.576
35	Loma Prieta	1989	Oakland - Outer Harbor Wharf	1825	1358	959.8	0.744	0.526
36	Loma Prieta	1989	Saratoga - Aloha Ave	3334	2504	1196	0.751	0.359
37	Erzican, Turkey	1992	Erzincan	7981	6867	4969	0.860	0.623
38	Cape Mendocino	1992	Petrolia	4631	3808	2046	0.822	0.442
39	Landers	1992	Barstow	1835	1456	1062	0.793	0.579
40	Landers	1992	Lucerne	21852	21319	11956	0.976	0.547
41	Landers	1992	Yermo Fire Station	5650	5308	3958	0.940	0.701
42	Northridge-01	1994	Jensen Filter Plant	7842	6530	5635	0.833	0.719
43	Northridge-01	1994	Jensen Filter Plant Generator	7869	6534	5625	0.830	0.715
44	Northridge-01	1994	LA-Wadsworth VA Hospital North	1118	566.7	303.8	0.507	0.272
45	Northridge-01	1994	LA Dam	3604	2392	1541	0.664	0.428
46	Northridge-01	1994	Newhall - W Pico Canyon Rd.	8977	7984	5841	0.889	0.651
47	Northridge-01	1994	Pacoima Dam (downstr)	820.7	411.6	235.4	0.501	0.287
48	Northridge-01	1994	Pacoima Dam (upper left)	5265	3233	2682	0.614	0.509
49	Northridge-01	1994	Rinaldi Receiving Sta	12279	8850	7313	0.721	0.596
50	Northridge-01	1994	Sylmar - Converter Sta	19938	13005	8695	0.652	0.436
51	Northridge-01	1994	Sylmar - Converter Sta east	8348	6071	4664	0.727	0.559
52	Northridge-01	1994	Sylmar - Olive view med FF	10067	7203	5560	0.715	0.552
53	Kobe, Japan	1995	Takarazuka	3716	2893	2107	0.778	0.567
54	Kobe, Japan	1995	Takatori	31747	18343	11261	0.578	0.355
55	Kocaeli, Turkey	1999	Gebze	4835	4383	3151	0.907	0.652
56	Chi-Chi, Taiwan	1999	CHY006	5585	3066	2090	0.549	0.374
57	Chi-Chi, Taiwan	1999	CHY035	2371	1297	865.1	0.547	0.365
58	Chi-Chi, Taiwan	1999	CHY101	12935	9017	6685	0.697	0.517
59	Chi-Chi, Taiwan	1999	TAP003	2371	1395	1162	0.588	0.490
60	Chi-Chi, Taiwan	1999	TCU029	9457	8277	7293	0.875	0.771

Table 5. The comparison between CSV of the actual record and the simulated pulse (continued).

No.	Event	Year	Station name	E_{Record} (cm^2/s)	E_{PR} (cm^2/s)	E_{Pulse} (cm^2/s)	$\frac{E_{\text{PR}}}{E_{\text{Record}}}$	$\frac{E_{\text{Pulse}}}{E_{\text{Record}}}$
61	Chi-Chi, Taiwan	1999	TCU031	11468	9321	8506	0.813	0.742
62	Chi-Chi, Taiwan	1999	TCU034	3445	3207	1978	0.931	0.574
63	Chi-Chi, Taiwan	1999	TCU036	11581	9185	7313	0.793	0.631
64	Chi-Chi, Taiwan	1999	TCU038	9329	6716	6164	0.720	0.661
65	Chi-Chi, Taiwan	1999	TCU040	7806	6720	5316	0.861	0.681
66	Chi-Chi, Taiwan	1999	TCU042	4941	3755	2990	0.760	0.605
67	Chi-Chi, Taiwan	1999	TCU046	3722	3438	3077	0.924	0.827
68	Chi-Chi, Taiwan	1999	TCU049	7657	6697	4833	0.875	0.631
69	Chi-Chi, Taiwan	1999	TCU053	5217	4229	3136	0.811	0.601
70	Chi-Chi, Taiwan	1999	TCU054	8964	7334	4504	0.818	0.502
71	Chi-Chi, Taiwan	1999	TCU056	5660	4663	2109	0.824	0.373
72	Chi-Chi, Taiwan	1999	TCU060	4034	3633	2366	0.901	0.587
73	Chi-Chi, Taiwan	1999	TCU065	48055	33512	23496	0.697	0.489
74	Chi-Chi, Taiwan	1999	TCU068	161270	151168	135657	0.937	0.841
75	Chi-Chi, Taiwan	1999	TCU075	17952	13447	9921	0.749	0.553
76	Chi-Chi, Taiwan	1999	TCU076	5995	3224	2398	0.538	0.400
77	Chi-Chi, Taiwan	1999	TCU082	9468	7376	4720	0.779	0.499
78	Chi-Chi, Taiwan	1999	TCU087	6287	5947	3710	0.946	0.590
79	Chi-Chi, Taiwan	1999	TCU098	4233	2564	1835	0.606	0.433
80	Chi-Chi, Taiwan	1999	TCU101	8733	7001	4263	0.802	0.488
81	Chi-Chi, Taiwan	1999	TCU102	19241	14996	8546	0.779	0.444
82	Chi-Chi, Taiwan	1999	TCU103	12068	10360	8953	0.859	0.742
83	Chi-Chi, Taiwan	1999	TCU104	4921	4055	3150	0.824	0.640
84	Chi-Chi, Taiwan	1999	TCU128	17524	14231	11969	0.812	0.683
85	Chi-Chi, Taiwan	1999	TCU136	7147	6277	4872	0.878	0.682
86	Northwest China-03	1997	Jiashi	542.6	421.5	316.5	0.777	0.583
87	Yountville	2000	Napa Fire Station #3	531	406.8	389.7	0.766	0.734
88	Chi-Chi, Taiwan-03	1999	CHY024	2244	1719	1250	0.766	0.557
89	Chi-Chi, Taiwan-03	1999	CHY080	3222	2982	2678	0.926	0.831
90	Chi-Chi, Taiwan-03	1999	TCU076	1012	886.6	711.3	0.876	0.703
91	Chi-Chi, Taiwan-06	1999	CHY101	2179	1474	1363	0.677	0.626

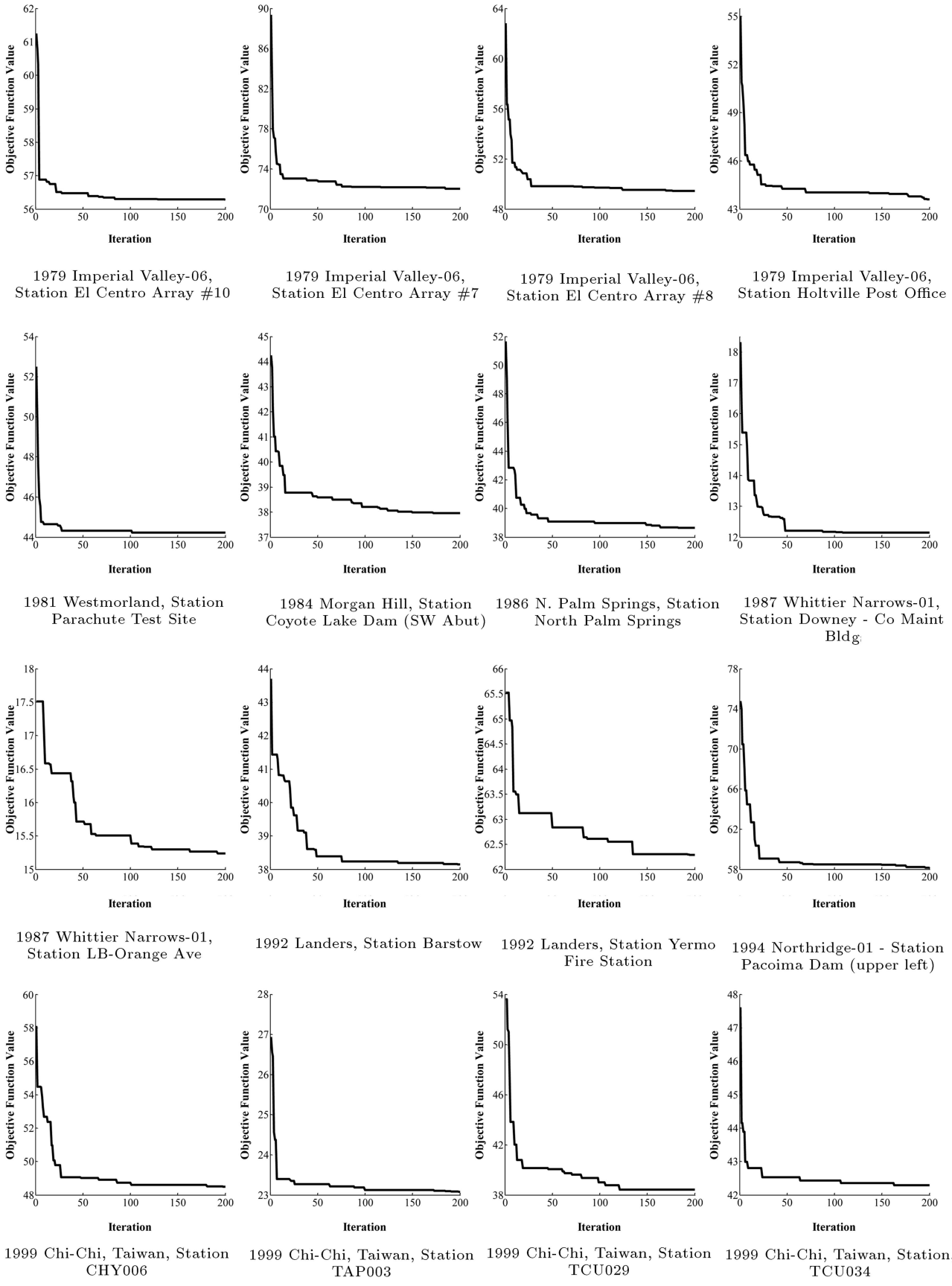

Figure 5. The convergence of the proposed approach.

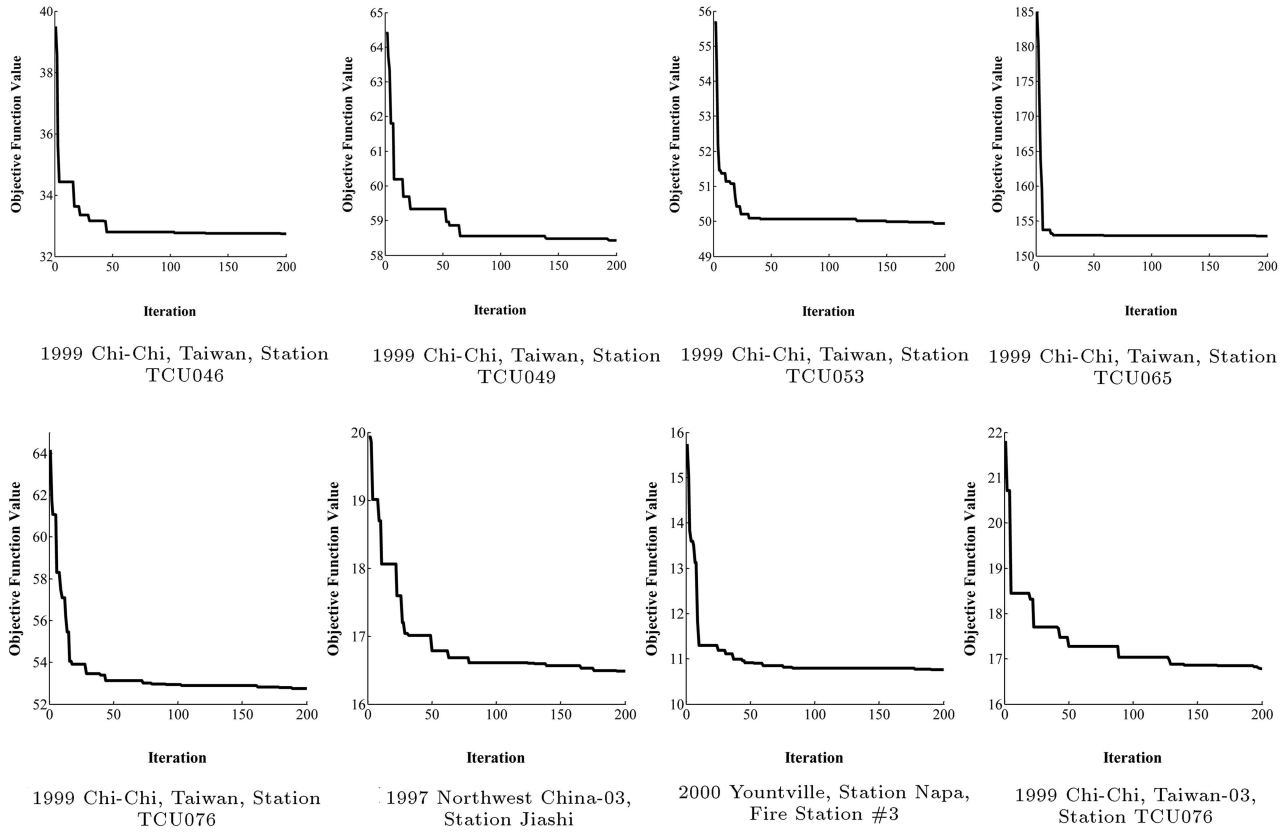

Figure 5. The convergence of the proposed approach (continued).

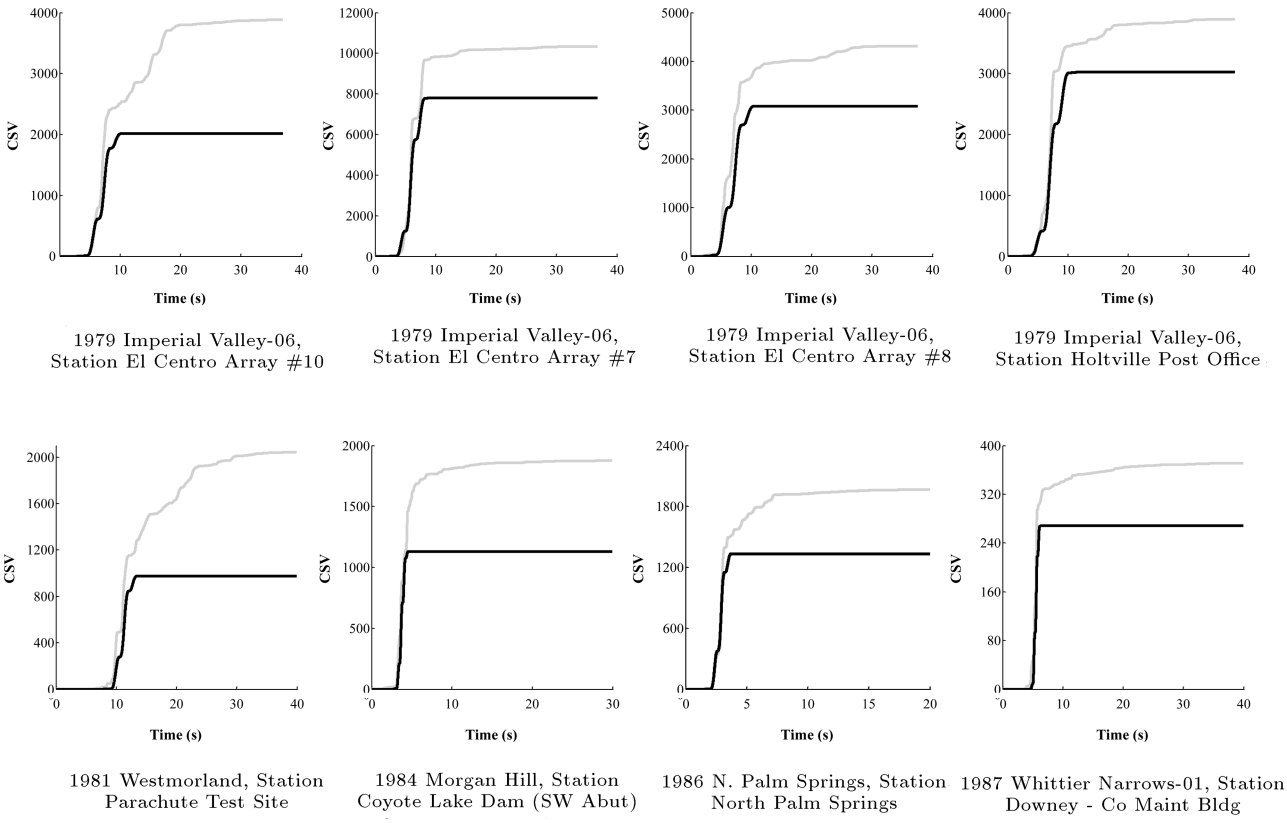

Figure 6. CSV of actual record (gray) and that of the simulated pulse (black).

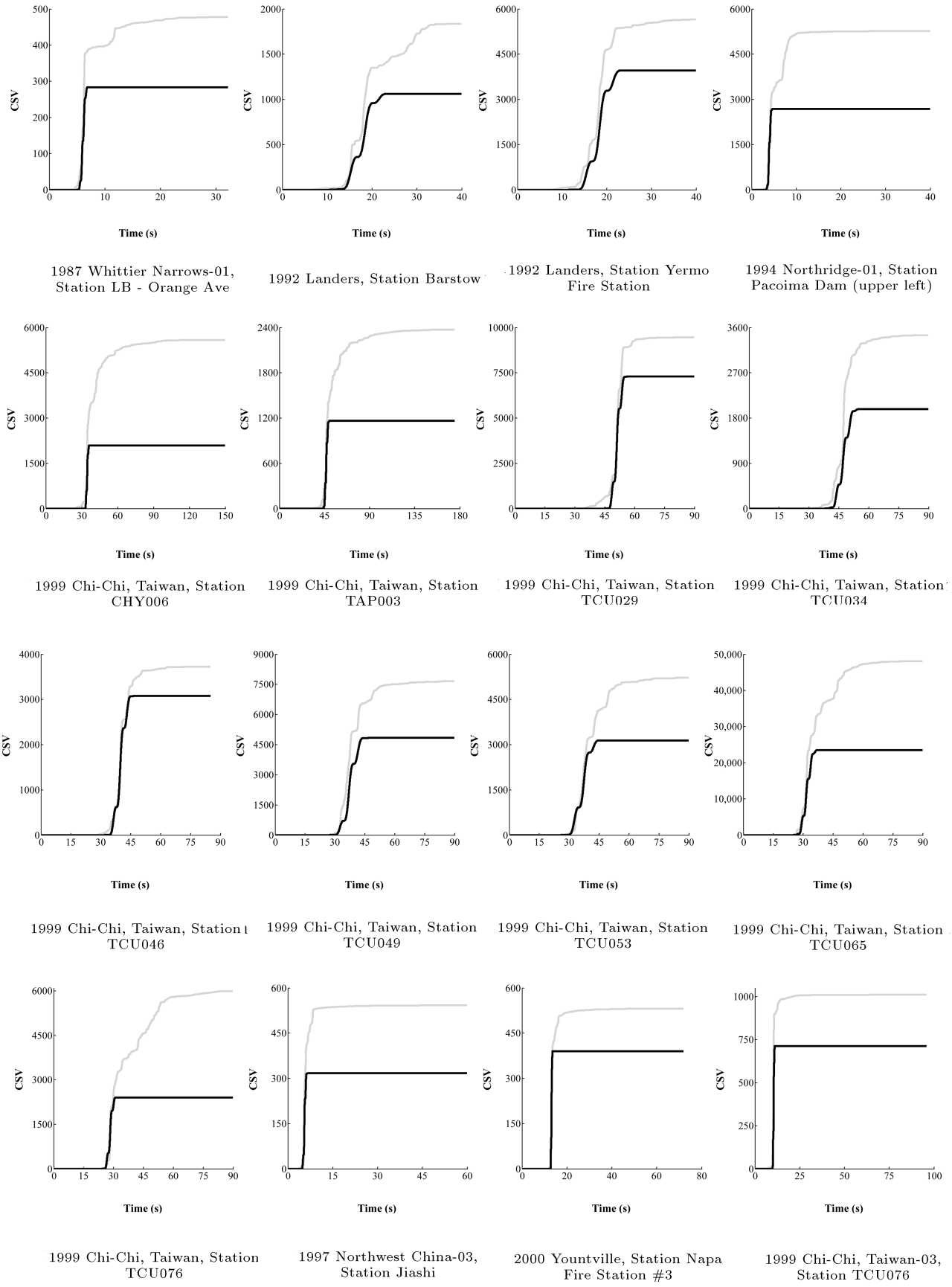

Figure 6. CSV of actual record (gray) and that of the simulated pulse (black) (continued).

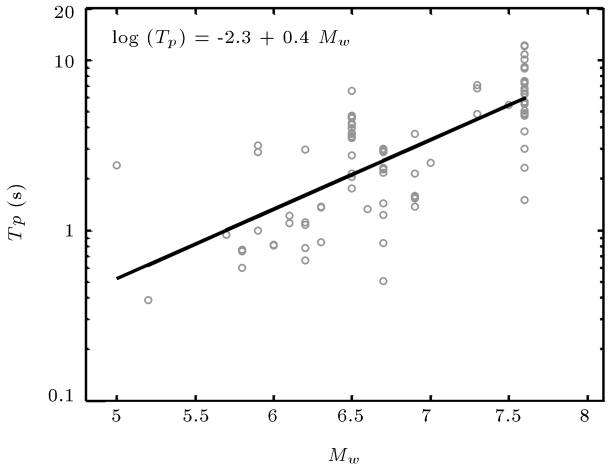

Figure 7. Linear regression of the prevalent pulse period and the earthquake magnitude.

5. Conclusion

Because of the destructive effects of near-fault earthquakesand pulse-like motions on structures and infrastructure, they have attracted special attention in seismology and earthquake engineering, and many analytical models have been presented to simulate such records. Some of these models are simple mathematical equations that use clear physical parameters to mathematically represent pulse-like records by simultaneously fitting time histories and response spectra of the actual records and the simulated pulses through a trial-and-error process. Such a process limits the ability of researchers and engineers to practically use the simulation model. Therefore, the trial-and-error process was replaced in this study by using constrained PSO algorithm. In addition, by applying penalty function, root-mean-square differences of time histories and response spectra of the actual records and simulated pulses were minimized simultaneously. Then, a set of 91 pulse-like records from NGA strong ground motion database was studied, and by choosing a mathematical model and using the proposed approach, the largest velocity pulse in this set was identified, extracted, and represented mathematically. The results are presented in a table of parameters. This information can help engineers study structure responses to pulse-like records. Moreover, the proposed approach can facilitate the extraction of any pulse-like record and its representation as closed mathematical equations. The recorded pulse history can be used for structural analysis and for studying structure responses to pulse-like motions.

References

1. Bertero, V.V., Mahin, S.A., and Herrera, R.A. "Aseismic design implications of near-fault San Fernando earthquake records", *Earthquake Engineering and Structural Dynamics*, **6**(1), pp. 31–42 (1978).

2. Anderson, J.C. and Bertero, V.V. "Uncertainties in establishing design earthquakes", *Journal of Structural Engineering*, **113**(8), pp. 1709–1724 (1987).

3. Hall, J.F., Heaton, T.H., Halling, M.W., and Wald, D.J. "Near-source ground motion and its effects on flexible buildings", *Earthquake Spectra*, **11**(4), pp. 569–605 (1995).

4. Iwan, W.D. "Drift spectrum: Measure of demand for earthquake ground motions", *Journal of Structural Engineering*, **123**(4), pp. 397–404 (1997).

5. Alavi, B. and Krawinkler, H., *Effects of Near-Fault Ground Motions on Frame Structures*, John A. Blume Earthquake Engineering Center Stanford (2001).

6. Menun, C. and Fu, Q. "An analytical model for near-fault ground motions and the response of SDOF systems", *Proceedings of 7th US National Conference on Earthquake Engineering*, Boston, Massachusetts, pp. 21–25 (2002).

7. Makris, N. and Black, C.J. *Dimensional Analysis of Inelastic Structures Subjected to Near Fault Ground Motions*, Earthquake Engineering Research Center, University of California (2003).

8. Akkar, S., Yazgan, U., and Gülkan, P. "Drift estimates in frame buildings subjected to near-fault ground motions", *Journal of Structural Engineering*, **131**(7), pp. 1014–1024 (2005).

9. Luco, N. and Cornell, C.A. "Structure-specific scalar intensity measures for near-source and ordinary earthquake ground motions", *Earthquake Spectra*, **23**(2), pp. 357–392 (2007).

10. Xie, L., Xu, L., and Adrian, R.M. "Representation of near-fault pulse-type ground motions", *Earthquake Engineering and Engineering Vibration*, **4**(2), pp. 191–199 (2005).

11. Zhai, C., Li, S., Xie, L., and Sun, Y. "Study on inelastic displacement ratio spectra for near-fault pulse-type ground motions", *Earthquake Engineering and Engineering Vibration*, **6**(4), pp. 351–355 (2007).

12. Ribakov, Y. "Reduction of structural response to near-fault earthquakes by seismic isolation columns and variable friction dampers", *Earthquake Engineering and Engineering Vibration*, **9**(1), pp. 113–122 (2010).

13. Yaghmaei-Sabegh, S. "Detection of pulse-like ground motions based on continues wavelet transform", *Journal of Seismology*, **14**(4), pp. 715–726 (2010).

14. Alonso-Rodríguez, A. and Miranda, E. "Assessment of building behavior under near-fault pulse-like ground motions through simplified models", *Soil Dynamics and Earthquake Engineering*, **79**, pp. 47–58 (2015).

15. Zhao, W.S. and Chen, W.Z. "Effect of near-fault ground motions with long-period pulses on the tunnel", *Journal of Vibroengineering*, **17**(2), pp. 841–858 (2015).

16. Alhan, C. and Öncü-Davas, S. "Performance limits of seismically isolated buildings under near-field earthquakes", *Engineering Structures*, **116**, pp. 83–94 (2016).

17. Alhan, C., Gazi, H., and Kurtuluş, H. "Significance of stiffening of high damping rubber bearings on the response of base-isolated buildings under near-fault earthquakes", *Mechanical Systems and Signal Processing*, **79**, pp. 297–313 (2016).

18. Chen, Z., Chen, W., Li, Y., and Yuan, Y. "Shaking table test of a multi-story subway station under pulse-like ground motions", *Soil Dynamics and Earthquake Engineering*, **82**, pp. 111–122 (2016).

19. Yazdani, Y. and Alembagheri, M. "Effects of base and lift joints on the dynamic response of concrete gravity dams to pulse-like excitations", *Journal of Earthquake Engineering*, **21**(5), pp. 840–860 (2017).

20. Zhao, G.C., Xu, L., and Xie, L. "Study on low-frequency characterizations of pulse-type ground motions through multi-resolution analysis", *Journal of Earthquake Engineering*, **20**(6), pp. 1011–1033 (2016).

21. Baker, J.W. "Quantitative classification of near-fault ground motions using wavelet analysis", *Bulletin of the Seismological Society of America*, **97**(5), pp. 1486–1501 (2007).

22. Mavroeidis, G.P. and Papageorgiou, A.S. "A mathematical representation of near-fault ground motions", *Bulletin of the Seismological Society of America*, **93**(3), pp. 1099–1131 (2003).

23. Hoseini-Vaez, S.R., Sharbatdar, M.K., Ghodrati-Amiri, G., Naderpour, H., and Kheyroddin, A. "Dominant pulse simulation of near fault ground motions", *Earthquake Engineering and Engineering Vibration*, **12**(2), pp. 267–278 (2013).

24. Mimoglou, P., Psycharis, I.N., and Taflampas, I.M. "Determination of the parameters of the directivity pulse embedded in near-fault ground motions and its effect on structural response", In *Computational Methods in Earthquake Engineering*, pp. 27–48 (2017).

25. Kaveh, A., Hoseini Vaez, S.R., and Hosseini, P. "MATLAB code for an enhanced vibrating particles system algorithm", *International Journal of Optimization in Civil Engineering*, **8**(3), pp. 401–414 (2018).

26. Kaveh, A., Hoseini Vaez, S.R., and Hosseini, P. "Modified dolphin monitoring operator for weight optimization of frame structures", *Periodica Polytechnica Civil Engineering*, **61**(4), pp. 770–779 (2017).

27. Hoseini Vaez, S.R. and Sarvdalir, S. "Reliability-based optimization of one-bay 2-D steel frame", *KSCE Journal of Civil Engineering*, **22**(7), pp. 2433–2440 (2018).

28. Kaveh, A., Hoseini Vaez, S.R., and Hosseini, P. "Enhanced vibrating particles system algorithm for damage identification of truss structures", *Scientia Iranica*, **26**(1), pp. 246–256 (2019).

29. Hoseini Vaez, S.R. and Fallah, N. "Damage detection of thin plates using GA-PSO algorithm based on modal data", *Arabian Journal for Science and Engineering*, **42**(3), pp. 1251–1263 (2017).

30. Kaveh, A., Hoseini Vaez, S.R., Hosseini, P., and Fallah, N. "Detection of damage in truss structures using simplified dolphin echolocation algorithm based on modal data", *Smart Structures and Systems*, **18**(5), pp. 983–1004 (2016).

31. Shi, Y. and Eberhart, R. "A modified particle swarm optimizer", *Proceedings of the 1998 IEEE International Conference on Evolutionary Computation*, pp. 69–73 (1998).

32. Eberhart, R. and Kennedy, J. "A new optimizer using particle swarm theory", *Proceedings of the Sixth International Symposium on Micro Machine and Human Science Nagoya*, Japan, pp. 39–43 (1995).

33. Kennedy, J. and Eberhart, R. "Particle swarm optimization", *Proceedings of the IEEE International Conference on Neural Networks Piscataway*, pp. 1942–1948 (1995).

34. Bazaraa, M.S., Sherali, H.D., and Shetty, C.M. "Nonlinear programming: Theory and algorithms", John Wiley & Sons, Canada, USA (2013).

35. Coello, C.A.C. "Theoretical and numerical constraint-handling techniques used with evolutionary algorithms: A survey of the state of the art", *Computer Methods in Applied Mechanics and Engineering*, **191**(11), pp. 1245–1287 (2002).

36. McFadden, P.D., Cook, J.G., and Forster, L.M. "Decomposition of gear vibration signals by the generalised S transform", *Mechanical Systems and Signal Processing*, **13**(5), pp. 691–707 (1999).

37. Trifunac, M.D. "Energy of strong motion at earthquake source", *Soil Dynamics and Earthquake Engineering*, **28**(1), pp. 1–6 (2008).

38. Todorovska, M.I., Meidani, H., and Trifunac, M.D. "Wavelet approximation of earthquake strong ground motion-goodness of fit for a database in terms of predicting nonlinear structural response", *Soil Dynamics and Earthquake Engineering*, **29**(4), pp. 742–751 (2009).

Appendix A

In Figure A.1, the actual record and extracted strong velocity pulse from 91 pulse-like records of Table 2 are shown. The complete fitting of the simulated pulse

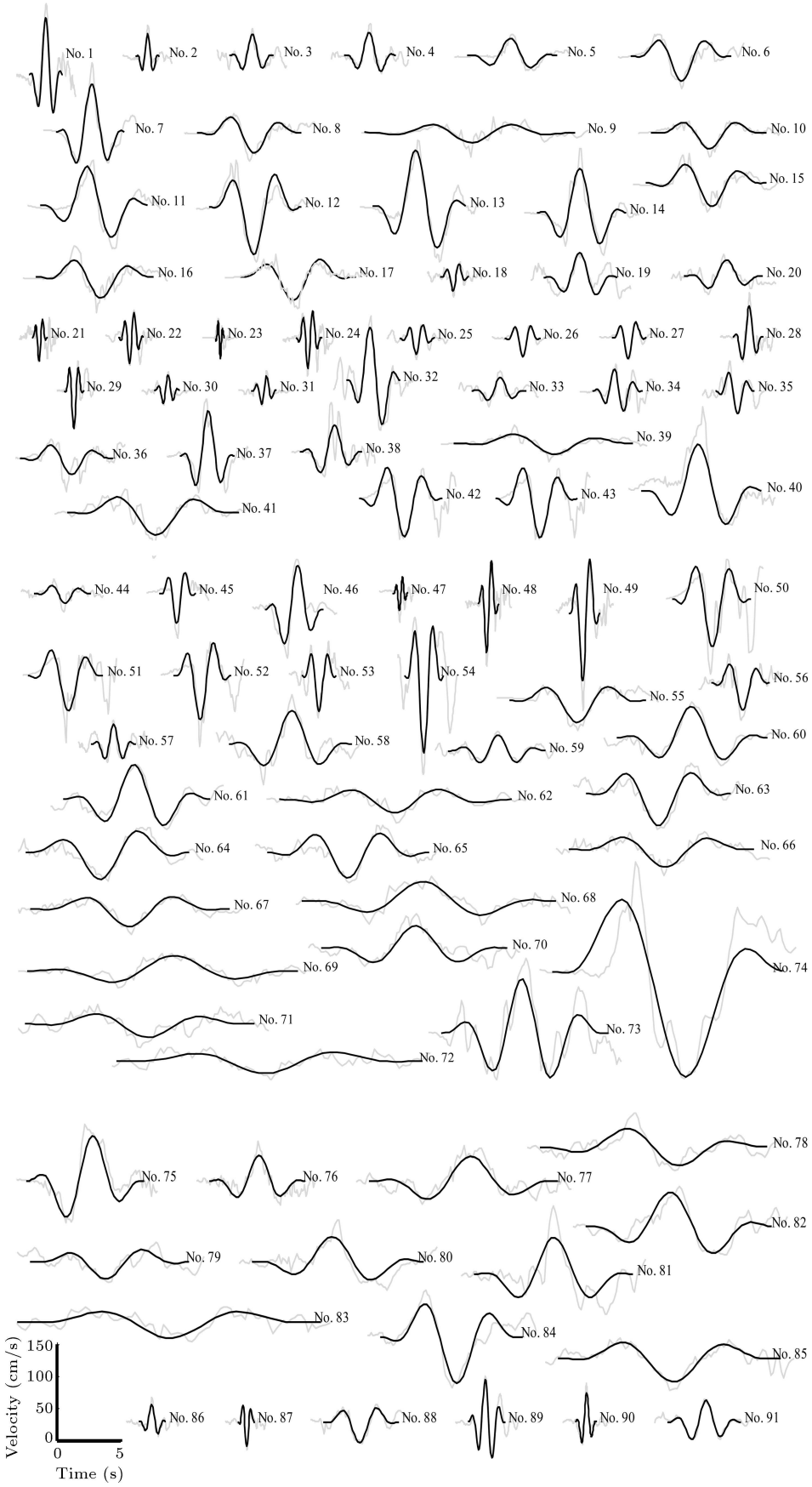

Figure A.1. Extracted strong velocity pulse and the original records of Table 2.

and the actual record is obtained by substituting the parameters of Table 4 in the analytical model of Hoseini Vaez et al. [23].

Biographies

Seyed Rohollah Hoseini Vaez is currently an Associate Professor at the University of Qom. He teaches courses on the finite element methods, structural optimization, advanced reinforced concrete structures, and earthquake engineering. His research interests include damage detection, finite element method, optimization algorithms, and near-fault ground motions.

Zahra Minaei graduated with an MSc degree in Civil Engineering, Structural Engineering, from Arak University, Arak, Iran in 2013, where she also received her BSc in 2010. She is currently a PhD candidate in Structural Engineering, at the University of Qom, Qom, Iran. Her research interests include seismic analysis, optimization methods, and fuzzy clustering approach.